RSC Advances

PAPER

View Article Online
View Journal | View Issue

Cite this: *RSC Adv.*, 2026, **16**, 14959

Phytochemical profiling of *Euphorbia tirucalli* Linn. latex and evaluation of its *in vitro* antibacterial activity against resistant *Klebsiella pneumoniae*: an integrative network pharmacology and molecular dynamics simulation study

Fathy A. Behery, †[ab] Abeer H. Elmaidomy,†[c] Rehab Mahmoud Abd El-Baky,[de] Mohamed A. Mawhoup,[e] Ruqaiah I. Bedaiwi,[f] Hesham A. Abou-Zied,[g] Mostafa E. Rateb[h] and Usama Ramadan Abdelmohsen*[ij]

A phytochemical investigation of *Euphorbia tirucalli* Linn. (F. Euphorbiaceae) latex resulted in the isolation of five known compounds, namely euphol (**1**), euph-8-enol (**2**), gallic acid (**3**), methyl gallate (**4**), and rutin (**5**). The chemical structures of the isolated compounds were unambiguously established by extensive nuclear magnetic resonance (NMR) spectroscopic analysis. The antimicrobial activities of these compounds were evaluated against *Klebsiella pneumoniae* (ATCC 13883), extended-spectrum β-lactamase (ESBL)-producing *K. pneumoniae*, and carbapenem-resistant *K. pneumoniae* using the microbroth dilution method. Among the tested compounds, methyl gallate (**4**) exhibited the strongest activity against *K. pneumoniae* (ATCC 13883) with a minimum inhibitory concentration (MIC) of 0.01 mM, while euphol (**1**) showed the highest activity against ESBL *K. pneumoniae* (MIC = 13.12 mM). Notably, euph-8-enol (**2**) demonstrated the most potent inhibitory effect against carbapenem-resistant *K. pneumoniae,* with an MIC of 0.69 mM. Network analysis identified 33 host-response targets relevant to *Klebsiella* infection, enriched in pattern-recognition receptor signaling and inflammatory defense programs, particularly the Toll-like receptor and NOD-like pathways, alongside cytokine/chemokine-mediated recruitment and inflammasome-associated signaling. Molecular docking against *Klebsiella pneumoniae* LpxH (PDB: 8QK2) showed the strongest predicted affinity for euphol (**1**) (−8.13 kcal mol^{-1}). MD simulation of the euphol (**1**)-LpxH complex over 100 ns supported overall system stability, evidenced by a stable protein backbone RMSD, maintained compactness (R_g), equilibrated potential energy, and intermittent hydrogen bonding consistent with predominantly hydrophobic binding. Collectively, these findings suggested that *E. tirucalli*, with euphol as the top-ranked binder, could provide structural starting points for further investigation for anti-*Klebsiella* development, warranting further *in vitro* validation of LpxH inhibition and antibacterial efficacy against resistant *Klebsiella* strains.

Received 27th January 2026
Accepted 9th March 2026

DOI: 10.1039/d6ra00720a

rsc.li/rsc-advances

1. Introduction

Euphorbiaceae is one of the largest and evolutionarily ancient angiosperm families, comprising approximately 300 genera and 8000 species, many of which produce latex.[1] The genus *Euphorbia* (spurge) is widely distributed across temperate and tropical regions and includes species of significant biological and medicinal importance.[1] A defining characteristic of *Euphorbia* species is the production of a white, acrid, and toxic

[a]*Department of Pharmacognosy, Faculty of Pharmacy, Mansoura University, Mansoura, Egypt. E-mail: fathybehery@mans.edu.eg*
[b]*Department of Pharmacy, College of Pharmacy, Nursing and Medical Sciences, Riyadh Elm University, Riyadh, Saudi Arabia*
[c]*Department of Pharmacognosy, Faculty of Pharmacy, Beni-Suef University, Beni-Suef 62514, Egypt. E-mail: Abeer011150@pharm.bsu.edu.eg*
[d]*Department of Microbiology and Immunology, Faculty of Pharmacy, Minia University, Minia, Egypt. E-mail: rehab.mahmoud@mu.edu.eg*
[e]*Department of Microbiology and Immunology, Faculty of Pharmacy, Deraya University, Minia, Egypt. E-mail: mohamed.mawhoup@deraya.edu.eg*
[f]*Department of Medical Laboratory Technology, Faculty of Applied Medical Sciences, University of Tabuk, Tabuk, Saudi Arabia. E-mail: rbedaiwi@ut.edu.sa*
[g]*Department of Medicinal Chemistry, Faculty of Pharmacy, Deraya University, Minia 61111, Egypt. E-mail: hisham.alaa@deraya.edu.eg*
[h]*Natural and Medical Sciences Research Center, University of Nizwa, P.O. Box 33, Birkat Al Mauz, Nizwa, Oman. E-mail: m.rateb@unizwa.edu.om*
[i]*Deraya Center for Scientific Research, Deraya University, New Minia, Egypt*
[j]*Department of Pharmacognosy, Faculty of Pharmacy, Minia University, Minia, Egypt. E-mail: usama.ramadan@mu.edu.eg*
† Authors equally contributed to this work.

milky latex that is released upon mechanical injury and causes severe skin irritation.[1] Phytochemical investigations of *Euphorbia* latex have revealed a diverse composition of bioactive compounds, including diterpenes, triterpenoids, ingenol derivatives, 12-deoxyphorbol esters, triterpene alcohols, lanosterol, fatty acids, proteins, and enzymes.[1] Terpenoids constitute the predominant chemical class and are primarily responsible for the pharmacological activities and therapeutic potential of the genus.[1]

Euphorbia tirucalli Linn. (Euphorbiaceae) is a temperate-region shrub or small tree characterized by slender, pencil-like branches. Phytochemical analyses have revealed the presence of sterols, triterpenoids, diterpenes, phenolic acids, and phorbol ester derivatives, including euphol, β-sitosterol, cycloartenol, taraxerol, β-amyrin, euphorbins, and tirucallins.[2] The species exhibits a broad spectrum of pharmacological activities, such as antimicrobial, anti-inflammatory, antioxidant, antiviral, anticancer, hepatoprotective, immunomodulatory, insecticidal, and central nervous system-related effects.[2]

Klebsiella pneumoniae is a Gram-negative, encapsulated, non-motile, facultatively anaerobic bacterium and a major opportunistic and iatrogenic pathogen.[3] While it can colonize the respiratory and gastrointestinal tracts asymptomatically, infection occurs under compromised immunity, such as in patients with diabetes, on glucocorticoid therapy, or post-transplant.[3] Susceptibility depends on pathogen virulence and antibiotic resistance, host intrinsic factors (genetics, age, immune status), and extrinsic factors including antibiotic use, environment, nutrition, and alcohol consumption.[4]

K. pneumoniae infections are managed with antibiotics guided by *in vitro* susceptibility, including cephalosporins, quinolones, or carbapenems.[5] However, resistance arises through β-lactamase production, membrane alterations, target modification, biofilm formation, efflux pumps, and integron acquisition, exacerbated by sublethal antibiotic exposure from clinical misuse or agricultural sources.[6] Extensive carbapenem use has promoted carbapenem-resistant *K. pneumoniae*, a major risk factor for nosocomial mortality, primarily *via* carbapenemases classified as Ambler class A (KPC), B (NDM, VIM, IMP), and D (OXA) enzymes.[7] Therefore, the development of novel anti-*Klebsiella pneumoniae* agents is urgently required, and plant-derived compounds represent a promising therapeutic strategy.

In the present study, five compounds were isolated and identified from *E. tirucalli* latex. The isolated compounds were evaluated for their anti-*Klebsiella pneumoniae* (ATCC 13883), extended-spectrum β-lactamase (ESBL)-producing *K. pneumoniae*, and carbapenem-resistant *K. pneumoniae* activities. Additionally, the structures of the isolated compounds were subjected to molecular docking to identify possible mechanisms underlying their activities.

2. Materials and methods

2.1. Plant material

E. tirucalli were collected in August 2024 from Faculty of Pharmacy, Beni-Suef, Egypt, kindly identified by Dr Abd El-Halim A. Mohammed of the Horticultural Research Institute, Department of Flora and Phytotaxonomy Research, Dokki, Cairo, Egypt. A voucher specimen (2024-DrPD 103) was deposited at the Department of Pharmacognosy, Faculty of Pharmacy, Deraya University, Egypt.

2.2. Chemicals and reagents

The solvents used in this work included *n*-hexane (*n*-hex., boiling point b.p. 60–80 °C), dichloromethane (DCM), ethyl acetate (EtOAc), and methanol (MeOH) were purchased from El-Nasr Company for Pharmaceuticals and Chemicals (Egypt). HPLC and deuterated solvents used for chromatographic and spectroscopic analyses were purchased from Sigma-Aldrich (Saint Louis, Missouri, USA), including chloroform ($CDCL_3$), methanol (CD_3OD), dimethyl sulfoxide (DMSO), HPLC-methanol, and HPLC-water. Column chromatography (CC) was performed using silica gel 60 (63–200 μm, E. Merck, Sigma-Aldrich). Thin-layer chromatography (TLC) was performed on pre-coated silica gel 60 GF_{254} plates (E. Merck, Darmstadt, Germany; 20 × 20 cm, 0.25 mm thick). Spots were visualized by spraying with *para*-anisaldehyde (PAA) reagent (absolute ethanol : sulfuric acid : glacial acetic acid : *para*-anisaldehyde) (85 : 5 : 10 : 0.5), followed by heating to 110 °C.[8]

2.3. Spectral analysis

At 400 and 100 MHz, respectively, proton ^1H and ^{13}C Distortionless Enhancement by Polarisation Transfer-Q (DEPT-Q) NMR spectra were captured. Tetramethylsilane (TMS) was used as an internal standard in chloroform ($CDCL_3$), methanol (CD_3OD), and dimethyl sulfoxide (DMSO) using the residual solvent peak ($\delta_H = 7.26$ and $\delta_C = 77.1$), ($\delta_H = 3.34$, 4.78 and $\delta_C = 49.9$) and $\delta_H = 2.50$ and $\delta_C = 39.5$, respectively) as references, respectively. The Bruker Advance III 400 MHz with BBFO Smart Probe and the Bruker 400 MHz AEON Nitrogen-Free Magnet were used for the measurements (Bruker AG, Billerica, MA, USA). Carbon multiplicities were determined using a DEPT-Q experiment.[9–16] The ultraviolet radiation (UV) spectrum in methanol was obtained using a Shimadzu UV 2401 PC spectrophotometer (Shimadzu Corporation – UV-2401PC/UV-2501PC, Kyoto, Japan). Infrared (IR) spectra were measured using a Jasco FTIR 300E infrared spectrophotometer. HRESIMS data were obtained using an Acquity Ultra Performance Liquid Chromatography system coupled with a Synapt G2 HDMS quadrupole time-of-flight hybrid mass spectrometer (Waters, Milford, MA, USA). HPLC chromatographic separations were conducted using an Agilent 1260 Infinity preparative pump (G1361 A), Agilent 1260 diode array detector VL (G1315 D), Agilent 1260 Infinity Thermostand column compartment (G1361 A), Agilent 1260 Infinity preparative autosampler (G2260 A) and a YMC-Pack ODS-A A-324 column (i.d. 10 × 300 mm, YMC, Kyoto, Japan.

2.4. Isolation and purification of compounds

Latex (3 g) was fractionated separately on polyamide-6 (column 50–160 μm, 1000 × 5 cm, 100 g) using gradient elution, starting with water (H_2O) and ending with MeOH in the order of

increasing polarities (0, 5, 10, 15, 20, 25, 30, 35, 40, 45, 50, 60, 80 and 100%, 1000 mL each, FR 5 mL min^{-1}). The effluents were collected in fractions (200 mL each); each fraction was concentrated and monitored by TLC using system EtOAC : G.A.A. : F.A. : H_2O 10 : 1 : 1 : 2 and PAA reagent. Similar fractions were grouped and concentrated under reduced pressure to also provide three sub-fractions F1–F3. F1 and 2 (100 mg, H_2O–MeOH 6 : 4, 400 mg, H_2O–MeOH 5 : 5, respectively) were further chromatographed separately on Sephadex LH_{20} (0.25–0.1 mm, 100 × 0.5 cm, 100 gm) eluted with MeOH, to afford compounds **3** (20 mg), **4** (30 mg), and **5** (3 mg). F3 (1 g, H_2O–MeOH 2 : 8) was fractionated on a silica gel column (65 × 1.5 cm, 50 g), and an elution was performed using *n*-hex.: EtOAC gradient mixtures in order of increasing polarities (0, 5, 10, 15, 20, 25, 30, 35, 40, 45, 50, 60, 80 and 100%, 250 mL each, FR 3 mL min^{-1}). The effluents were collected in fractions (20 mL each); each fraction was concentrated and monitored by TLC to afford compounds **1** (20 mg), and **2** (7 mg).[9–16] The final purity of the isolated compounds was confirmed by analytical HPLC (C18 column, MeOH : H_2O 90 : 10, isocratic), at 210 nm, Fig. S1 and S2. Compound structures were confirmed by 1D and 2D NMR.

Euphol (**1**): white amorphous powder. The NMR parameters were ^{13}C NMR (100 MHz, $CDCl_3$): 15.7 (C29), 15.8 (C18), 17.8 (C26), 19.0 (C21), 19.0 (C6), 20.2 (C19), 21.6 (C11), 24.6 (C30), 24.8 (C23), 25.8 (C27), 27.8 (C2, C7), 27.9 (C28), 28.1 (C16), 29.8 (C15), 31.0 (C12), 35.4 (C1), 35.5 (C22), 35.9 (C20), 37.3 (C10), 39.0 (C4), 44.2 (C13), 49.7 (C17), 50.1 (C14), 51.0 (C5), 79.1 (C3), 125.3 (C24), 130.8 (C25), 133.6 (C9), 134.1 (C8) and ^1H NMR (400 MHz, $CDCl_3$): 0.75 (3H, s, H-18), 0.80 (3H, s, H-29), 0.85 (3H, d, H-21), 0.87 (3H, s, H-30), 0.95 (3H, s, H-19), 1.00 (3H, s, H-28), 1.50 (3H, s, H-26), 1.68 (3H, s, H-27), 3.27 (1H, dd, H-3) and 5.30 (1H, bt, H-24). The tetracyclic triterpene euphol isolated in this study showed >95% purity. HR-ESI-MS *m*/*z* 427.3942 $[M + H]^+$ (calc. for $C_{30}H_{51}O$, 427.3940).

Euph-8-enol (**2**): white amorphous powder. The NMR parameters were ^{13}C NMR (100 MHz, $CDCl_3$): 15.7 (C29), 15.8 (C18), 17.8 (C26), 19.0 (C21), 19.0 (C6), 20.2 (C19), 21.6 (C11), 24.6 (C30), 24.8 (C23), 25.8 (C27), 27.8 (C2, C7), 27.9 (C28), 28.1 (C16), 28.2 (C24), 29.8 (C15), 31.0 (C12), 33.4 (C25), 35.4 (C1), 35.5 (C22), 35.9 (C20), 37.3 (C10), 39.0 (C4), 44.2 (C13), 49.7 (C17), 50.1 (C14), 51.0 (C5), 79.1 (C3), 133.6 (C9), 134.1 (C8) and ^1H NMR (400 MHz, $CDCl_3$): 0.75 (3H, s, H-18), 0.80 (3H, s, H-29), 0.85 (3H, d, H-21), 0.87 (3H, s, H-30), 0.95 (3H, s, H-19), 1.00 (3H, s, H-28), 1.50 (3H, s, H-26), 1.68 (3H, s, H-27), and 3.27 (1H, dd, H-3). The tetracyclic triterpene euph-8-enol isolated in this study showed >95% purity. HR-ESI-MS *m*/*z* 429.4099 $[M + H]^+$ (calc. for $C_{30}H_{53}O$, 429.4096).

Gallic acid (**3**): yellowish-amorphous powder; UV (MeOH) λ_{max} (log ε) 270 (6.0) nm; IR υ_{max} (KBr) 3300, 1681, 1677, 1617, 1540, and 1451 cm^{-1}. The NMR parameters were ^{13}C NMR (100 MHz, DMSO): 109.9 (C2, C6), 113.2 (C1), 136.7 (C4), 148.9 (C3, C5), 159.9 (COOH), ^1H NMR (400 MHz, DMSO): 3.40 (sa, 4H, OH-4), 7.42 (s, 2H, H-2, H-6). HR-ESI-MS *m*/*z* 171.0295 $[M + H]^+$ (calc. for $C_7H_7O_5$, 171.0293).

Methyl gallate (**4**): yellowish-amorphous powder; UV (MeOH) λ_{max} (log ε) 270 (6.0) nm; IR υ_{max} (KBr) 3300, 1681, 1677, 1617, 1540, and 1451 cm^{-1}. The NMR parameters were ^{13}C NMR (100 MHz, CD_3OD): 52.3 (CH_3O–), 110.1 (C2, C6), 121.4 (C1), 139.7 (C4), 146.4 (C3, C5), 169.0 (CO), ^1H NMR (400 MHz, CD_3OD): 3.85 (s, 3H, CH_3–O), 7.06 (s, 2H, H-2, H-6). HR-ESI-MS *m*/*z* 185.0455 $[M + H]^+$ (calc. for $C_8H_9O_5$, 185.0450).

Rutin (**5**): yellowish-amorphous powder; UV (MeOH) λ_{max} (log ε) 256 (5.0), 355 (6.0) nm; IR υ_{max} (KBr) 3300, 1700, 1617, 1506, and 1013 cm^{-1}. The NMR parameters were ^{13}C NMR (100 MHz, CD_3OD): 17.9 (C6‴), 62.8 (C6″), 69.7 (C5‴), 71.4 (C4″), 72.0 (C2‴), 72.3 (C3‴), 74.0 (C4‴), 74.6 (C2″), 77.1 (C5″), 77.7 (C3″), 97.1 (C8), 97.9 (C6), 101.0 (C1‴), 102.0 (C1″), 105.8 (C10), 112.6 (C2′), 114.5(C5′), 119.1 (C6′), 122.9 (C1′), 132.8 (C3), 147.6 (C4′), 149.3 (C3′), 164.3 (C9), 164.9 (C2), 166.7 (C5), 166.8 (C7), and 175.3 (C4). ^1H NMR (400 MHz, CD_3OD): 1.28 (d, 3H, C6‴), 3.58, 3.70, (m, 2H, C6‴), 4.32 (d, 1H, C1″), 5.35 (s, 1H, C1‴), 6.16 (d, 1H, C6), 6.32 (d, 1H, C8), 6.91 (d, 1H, C5′), 7.34 (d, 1H, C6′), 7.35 (d, 1H, C2′). HR-ESI-MS *m*/*z* 611.1614 $[M + H]^+$ (calc. for $C_{27}H_{31}O_{16}$, 611.1612).

2.5. Bacterial strains and growth conditions

Standard *Klebsiella pneumoniae* (ATCC 13883), carbapenem-resistant *K. pneumoniae*, and ESBL *K. pneumoniae* were obtained from the department of Microbiology and Immunology, Faculty of Medicine, Tanta University, and stored at −80 °C in 2.5 M glycerol until use. For experimental assays, the strain was routinely cultured on Mueller–Hinton agar and grown in Mueller–Hinton broth at 37 °C for 18–24 h under aerobic conditions before each experiment.

2.6. Antimicrobial activity of the tested compounds against *K. pneumoniae* strains

2.6.1. Screening for the antimicrobial activity against *K. pneumoniae* tested strains. The antibacterial activity assay was done using the reported method.[17] The plates were prepared by pouring nutrient agar into sterile Petri dishes and allowing them to set. The microorganism was inoculated on the plates using a swab stick. A 4 mm cork borer was used to bore holes in the medium, and the bottom of each hole was sealed with a drop of molten agar to avoid leakage of the extract. Four holes were made in each Petri plate, adequately spaced out. About 0.2 μL of the different concentrations of each tested compound, crude extract and gentamicin were introduced into the well. The Petri plates were incubated at 37 °C for 24 h, after which the inhibition zones were measured using a ruler. All tested compounds were dissolved in DMSO at a final concentration ≤1% (v/v). Solvent-only controls were included in all assays and showed no observable antibacterial activity.

2.6.2. Determination of minimum inhibitory concentrations of the tested compounds. The broth microdilution method was used to determine the effect of *E. tirucalli* latex isolated compounds on different strains of *Klebsiella pneumoniae* (ATCC 13883), Extended Spectrum Beta-lactamase *Klebsiella pneumoniae*, and Carbapenem-resistant *Klebsiella pneumoniae*. The assay was performed in sterile 96-well plates, following the CLSI guideline M07 and ISO 20776-1, with minor modifications.[18] Serial twofold dilutions of the tested compounds (1000–1.95 μg mL^{-1}) were prepared in Muller–

Hinton broth (MHB), and 100 μL of each dilution was dispensed into wells. A 10 μL of freshly prepared suspension of the tested strains (1.5×10^7 CFU mL^{-1}) was placed in each well. Plates were inoculated within 15 min of preparation and incubated at 37 °C for 18–24 h. Negative control wells contained broth only, while positive-control wells contained inoculated broth without the tested compounds. Results were compared to the antibacterial activity of Amikacin. The experiment was done in triplicate. The presence (or absence) of growth was visually observed after the proper incubation period. The MIC was defined as the lowest concentration that visibly inhibited bacterial growth, taking into account the formation of cell clusters or "buttons" in the plate wells. To ensure clarity and consistency between the experimental dilution range and the reported results, MIC values were also converted between μg mL^{-1} and mM using the molecular weight (MW) of each compound. The conversion was calculated using the following equation:

$$\text{mM} = (\text{mg mL}^{-1} \times 1000) \div \text{MW}.$$

All MIC determinations were performed in three independent experiments, and the results are reported as the mean ± standard deviation (SD).

2.6.3. Statistical analysis. The data were tabulated using GraphPad Prism version 9 (GraphPad, La Jolla, CA, USA). All experiments were performed at least three times. $*p < 0.05$, Student's *t*-test. Regarding the antimicrobial assay, the assay was performed in three independent experiments. MIC values were determined as the lowest concentration that completely inhibited visible bacterial growth and are reported as mean ± standard deviation (SD) from triplicate experiments.

2.7. Protein–protein interaction network analysis

To investigate the potential anti-*Klebsiella* activity of *E. tirucalli* L. through a host-response modulation framework, a network pharmacology workflow was applied to a curated panel of 33 human proteins implicated in the immune and inflammatory response to *Klebsiella* infection. Predicted associations between major *E. tirucalli* phytoconstituents and the selected host targets were evaluated using the STITCH database to generate a compound–target interaction network. Subsequently, a protein–protein interaction (PPI) network was constructed using the STRING platform to characterize functional connectivity among these host-response proteins and to identify highly connected hub nodes. Network visualization and topological analysis were performed in Cytoscape.[19,20]

2.8. Functional annotation and pathway enrichment

To explore the biological roles of the identified host-response targets, Gene Ontology (GO) and KEGG pathway enrichment analyses were performed to characterize overrepresented functions across biological processes, molecular functions, and cellular components. The enrichment profile provided mechanistic insight into how *E. tirucalli* constituents may influence host pathways relevant to Gram-negative bacterial infection.

2.9. Molecular docking simulation

Docking studies were conducted to examine the binding affinities of *E. tirucalli*-derived compounds toward *K. pneumoniae* LpxH (PDB: 8QK2). The receptor and ligands were converted to the required docking format and prepared for docking (adding polar hydrogens, assigning partial charges, and removing non-essential heteroatoms as appropriate). The docking grid was defined around the catalytically relevant pocket. Docking was performed using AutoDock Vina v1.2.5 after receptor and ligand preparation for the PDBQT format, including addition of polar hydrogens, assignment of Gasteiger partial charges, and definition of AutoDock atom types. Protein–ligand interactions and 2D/3D binding mode visualizations were generated using BIOVIA Discovery Studio Visualizer.

2.10. Molecular dynamics (MD) simulations

To assess the stability of the ligand–protein complex, molecular dynamics (MD) simulations were performed using GROMACS 2023 on the top-ranked docking pose of euphol (**1**) bound to *K. pneumoniae* LpxH (PDB: 8QK2).[21] The CHARMM36 and CGenFF force fields were applied to the protein and ligands, respectively.[22] The complex was embedded in a TIP3P water box with a 1 nm buffer, and the system was neutralized using NaCl to achieve a 150 mM ionic concentration. Following energy

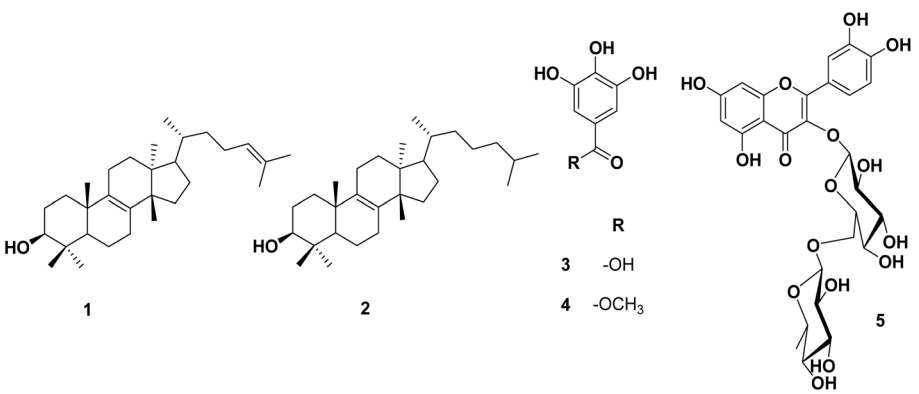

Fig. 1 Structures of compounds isolated from *E. tirucalli*.

minimization *via* the steepest descent method, equilibration was conducted under NVT and NPT ensembles for 100 ps each at 300 K and 1.0 bar, applying positional restraints. A 100 ns production run was then performed without restraints, and trajectories were recorded at 10 ps intervals. Analyses, including RMSD and binding energy evaluations, confirmed the structural stability of the complexes.

3. Results and discussion

3.1. Phytochemical investigation of *Euphorbia tirucalli*

Based on-the physicochemical, chromatographic-properties, the-spectral-analyses-from UV, ^{1}H, and-DEPT-Q, as well as-compared-with the-literature, the latex of *E. tirucalli* afforded the known euphol (**1**),[23] along with euph-8-enol (**2**),[23] gallic acid

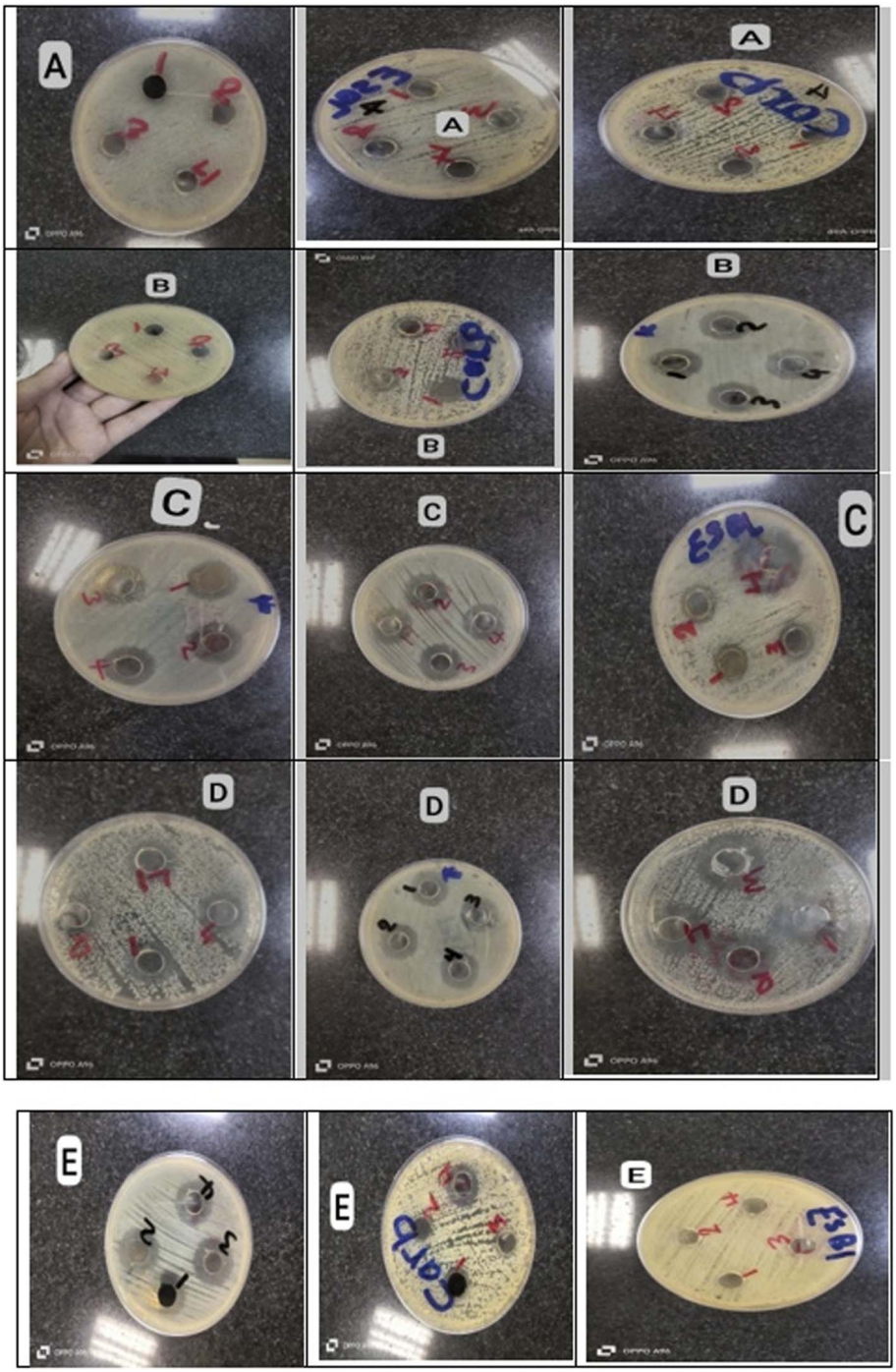

Fig. 2 Antibacterial activity of the tested compounds **1**–**5** and the extract against the tested *Klebsiella pneumoniae* strains (ATCC 13883, ESBL-producing, and carbapenem-resistant). The effect of 2-fold dilutions of the tested samples, serially diluted from **1** (the highest concentration) to **4** (the lowest concentration). (A) Compound **1** (euphol); (B) compound **2** (euph-8-enol); (C) compound **3** (gallic acid); (D) compound **4** (methyl gallate); and (E) compound **5** (rutin).

Table 1 Minimum inhibitory concentrations of the tested compounds isolated from *E. tirucalli* latex against different *K. pneumoniae* strains, as determined using the microbroth dilution method

MIC (mM)±SD[a]			
	Klebsiella pneumoniae (ATCC 13883)	ESBL *K. pneumoniae*	Carbapenem-resistant *K. pneumoniae*
1	0.23 ± 0.03	13.12 ± 0.43	25.77 ± 1.32
2	3.73 ± 0.26	23.32 ± 1.01	0.69 ± 0.23
3	0.07 ± 0.002	58.78 ± 1.65	35.26 ± 1.21
4	0.01 ± 0.00	54.30 ± 0.56	54.30 ± 2
5	20.47 ± 0.18	16 ± 0.92	16 ± 0.69
Amikacin	0.0034 ± 0.001	0.0273 ± 0.002	0.0546 ± 0.008

[a] MIC values were interpreted as mean ± SD (standard deviation).

(**3**),[24] methyl gallate (**4**),[24] and rutin (**5**),[25] (Fig. 1 and S3–S12). The characterized compounds (**2–5**) were isolated herein for the first time from these species.[1]

3.2. Screening of the antibacterial activity of the tested compounds against the tested *Klebsiella* strains

Screening of the anti-*Klebsiella* activity of the five compounds was performed using the well agar diffusion method, starting from 100 μM to 12.55 μM. Compound 1 showed the highest activity, with zone diameters ranging from 26 mm to 18 mm at the lower concentration. In contrast, the other tested compounds showed smaller zones of inhibition at the same concentration (Fig. 2).

3.3. Determination of the minimum inhibitory concentration of the tested compounds against the tested *Klebsiella* strains

In this investigation, the isolated compounds from *E. tirucalli* latex (compounds **1–5**), were evaluated against *K. pneumoniae* (ATCC 13883), ESBL *K. pneumoniae*, and carbapenem-resistant *K. pneumoniae* using the microbroth dilution method. The results showed that methyl gallate (**4**) (MIC = 0.01 mM), and euphol (**1**) (MIC = 13.12 mM), were the most effective against *K. pneumoniae* (ATCC 13883), and ESBL *K. pneumoniae*, respectively. While euph-8-enol (**2**) (MIC = 0.69 mM), showed the highest activity against carbapenem-resistant *K. pneumoniae*. Amikacin was used as a positive control (Table 1).

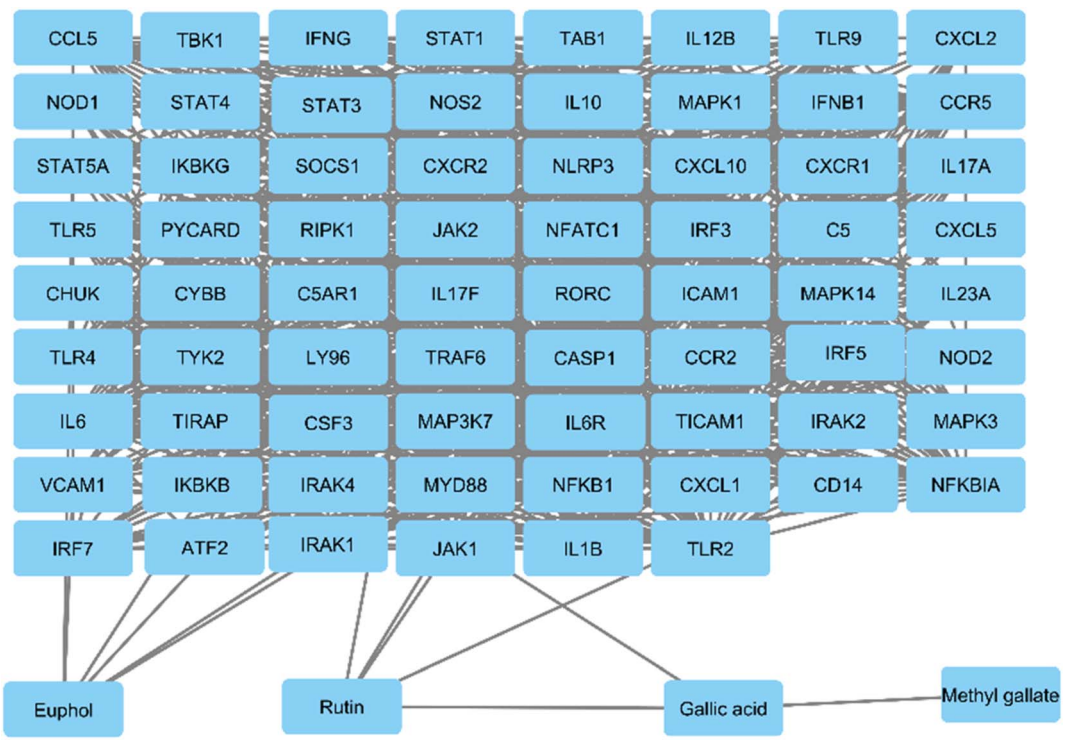

Fig. 3 STITCH network showing predicted interactions between *E. tirucalli* metabolites (euphol, rutin, gallic acid, methyl gallate) and human host-response targets relevant to *Klebsiella* infection, including TLR4/CD14–MYD88 signaling, NF-κB/MAPK/JAK–STAT pathways, cytokines/chemokines, inflammasome components, complement, and oxidative defense nodes.

It should be noted that several MIC values obtained in this study fall within the millimolar range, indicating relatively modest antibacterial potency in their current form. However, the objective of the present work was not to identify optimized antibacterial agents, but rather to explore bioactive natural product scaffolds that demonstrate measurable activity against clinically relevant resistant *Klebsiella* strains. Such natural metabolites often serve as initial hit structures that can be further optimized through medicinal chemistry approaches. Therefore, the compounds identified in this study should be considered preliminary structural frameworks that may guide future optimization rather than fully developed antibacterial leads.

Regarding previous results, the apparent discrepancy between agar diffusion results and MIC values may be attributed to differences in compound diffusion behavior in agar media. Diffusion-based assays are strongly influenced by physicochemical properties such as molecular size, polarity, and lipophilicity. Larger and more hydrophobic molecules may diffuse poorly through the agar matrix, producing smaller inhibition zones despite measurable antibacterial activity in broth-based assays. In contrast, smaller and more polar compounds may diffuse more easily and generate larger inhibition zones. Therefore, while agar diffusion assays were used as a preliminary qualitative screening method, MIC values determined by broth microdilution represent the more reliable measure of intrinsic antibacterial potency.

3.4. Protein–protein interaction (PPI) network analysis

3.4.1. Target identification for *Klebsiella* infection (Host–Human response). A total of 33 human host target proteins implicated in the immune and inflammatory response to *Klebsiella* infection were curated and consolidated (SI Table S1) to support downstream interaction and pathway analyses. This target panel was defined to reflect the dominant host-defense mechanisms against Gram-negative bacterial challenge, spanning: LPS recognition and innate sensing (*e.g.*, TLR4–CD14–LY96), proximal adaptor signaling (*e.g.*, MYD88, TICAM1, IRAK1/4, TRAF6), and downstream inflammatory transcriptional programs that regulate cytokine and chemokine production. In addition, the list includes key mediators of neutrophil recruitment (CXCL1/2/5 and CXCR1/2), inflammasome activation and IL-1β maturation (NLRP3, PYCARD, CASP1), Th17/IL-17 axis signaling (IL23A, IL17A, IL17F), complement activation (C3, C5, C5AR1), and oxidative antimicrobial effector responses (NOS2, CYBB, MPO), together with endothelial activation markers (ICAM1, VCAM1, SELP). The 33-host target panel was curated as a mechanistically focused seed set spanning LPS recognition/innate sensing, adaptor signaling, inflammatory cytokine and chemokine regulation, inflammasome activation, and complement/oxidative antimicrobial defense, and STITCH interaction mapping was performed using a high-confidence cutoff (confidence score ≥ 0.700) to prioritize more reliable predicted associations. Collectively, these host targets represent mechanistically relevant nodes through which bioactive compounds may modulate bacterial infection-associated inflammation and immune clearance, forming the basis for subsequent PPI construction and hub/pathway prioritization.

3.4.2. Interaction mapping of *E. tirucalli* compounds with *Klebsiella*-related host proteins. To evaluate the interaction potential of *E. tirucalli* L. latex bioactive constituents against

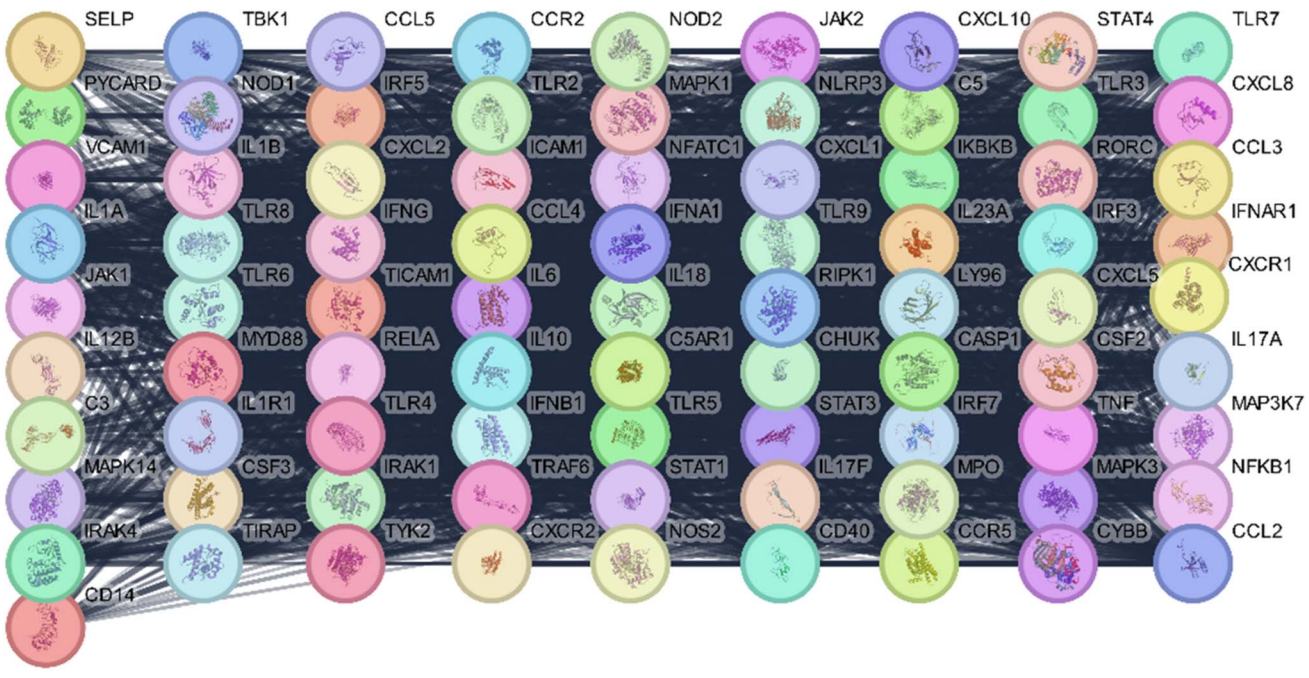

Fig. 4 STRING-derived PPI network of human host-response targets relevant to *Klebsiella* infection, highlighting interconnected innate sensing (TLR4/CD14/LY96–MYD88), NF-κB/MAPK signaling, cytokine/chemokine modules, inflammasome components, complement, and oxidative defense nodes.

host-response targets relevant to *Klebsiella* infection, key metabolites (euphol, rutin, gallic acid, and methyl gallate) were analyzed using the STITCH platform. The resulting interaction network (Fig. 3) depicts direct and indirect associations between these phytoconstituents and a host protein panel enriched for Gram-negative bacterial sensing and downstream inflammatory signaling, including LPS recognition and proximal innate activation (TLR4, CD14, LY96, MYD88, IRAK1/4, TRAF6, TICAM1/TIRAP), central transcriptional and kinase hubs (NFKB1, MAPK1/MAPK3/MAPK14, CHUK, IKBKB, JAK1/JAK2, STAT1/STAT3), and key effector outputs of antibacterial inflammation such as pro-inflammatory cytokines (IL1B, IL6, IL12B, IL23A, IFNG), neutrophil-recruiting chemokines and receptors (CXCL1, CXCL2, CXCL5, CXCL10; CXCR1, CXCR2), and inflammasome-related components (NLRP3, PYCARD, CASP1). The network also highlights nodes linked to complement and inflammatory amplification (C5, C5AR1) and oxidative antimicrobial mechanisms (NOS2, CYBB), reflecting host pathways commonly engaged during severe Gram-negative infections. Overall, these interaction patterns support a mechanistic premise that *E. tirucalli* metabolites may contribute to anti-*Klebsiella* activity by modulating host inflammatory circuitry and leukocyte-recruitment programs rather than antibacterial-specific pathways. Notably, euphol showed prominent connectivity to inflammatory and signaling mediators (*e.g.*, JAK2 and IL1B). At the same time, phenolic constituents (gallic acid and methyl gallate) and rutin displayed associations across cytokine/chemokine and innate signaling nodes, consistent with a multi-target immunomodulatory profile within the host-response network.

3.4.3. Construction of protein–protein interaction (PPI) network. To further investigate the functional crosstalk among human host-response targets relevant to *Klebsiella* infection and the putative immunomodulatory footprint of *E. tirucalli* L. constituents, a protein–protein interaction (PPI) network was generated using the STRING database (v12.0) and visualized in Cytoscape (v3.10.1). The resulting network formed a densely connected interactome (82 nodes, 2197 edges; average node degree: 53.56), consistent with coordinated activation of innate immune and inflammatory signaling during Gram-negative infection. In the subsequent STRING analysis, the 33 curated host proteins were used as the seed/query list; the exported PPI network expanded to 82 nodes because, in addition to the original seed proteins, STRING retained 49 additional first-shell interacting proteins supported by known/predicted functional associations, thereby capturing broader pathway connectivity within the host-response interactome. As shown in Fig. 4, highly connected hubs were enriched within LPS/innate sensing and adaptor signaling (*e.g.*, TLR4, CD14, LY96, MYD88, IRAK1/4, TRAF6, TICAM1), downstream NF-κB/MAPK and kinase signaling modules (*e.g.*, NFKB1, RELA, IKBKB, CHUK, MAPK1, MAPK3, MAPK14), and major inflammatory effector outputs including cytokines/chemokines and recruitment axes (*e.g.*, IL6, TNF, IL1B, CXCL8, CXCL1/2/5/10, CCR2, CXCR1/2). Additional connectivity was observed across inflammasome components (NLRP3, PYCARD, CASP1), complement amplification (C3, C5, C5AR1), and oxidative antimicrobial defense nodes (NOS2, CYBB, MPO). Collectively, the network topology supports a mechanistic framework in which *E. tirucalli* metabolites may influence anti-*Klebsiella* outcomes through multi-target modulation of innate immune activation, inflammatory amplification, leukocyte recruitment, and antibacterial effector pathways.

To prioritize the most influential proteins within the host-response interaction network relevant to *Klebsiella* infection, the CytoHubba plugin in Cytoscape was applied using the Maximal Clique Centrality (MCC) algorithm. This analysis identified the top 15 hub genes (Fig. 5) that occupy central positions across Gram-negative innate sensing, inflammatory amplification, and effector signaling. The highest-ranking nodes were enriched for TLR-driven activation and adaptor signaling (*e.g.*, TLR4, MYD88, TLR2, TLR9), core inflammatory cytokines (IL1B, IL6, TNF, IL1A, IL18), and key transcriptional/inflammatory regulators (NFKB1, CASP1). Additional hubs included CXCL8 (neutrophil recruitment) and cytokine modulators (IL10, IFNG), reflecting coordinated host programs implicated in antibacterial defense and immunopathology during *Klebsiella* infection. Overall, the dense interconnectivity of these hub proteins supports their potential as principal nodes through which *E. tirucalli* metabolites could modulate host inflammatory pathways associated with *Klebsiella* infection outcomes.

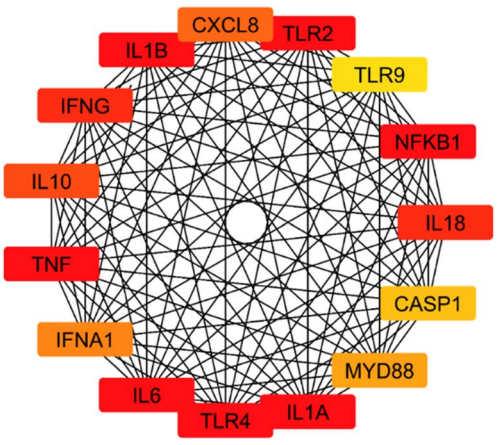

Fig. 5 CytoHubba (MCC) hub-gene network of the *Klebsiella*-relevant host-response PPI, highlighting the top 15 central nodes (*e.g.*, TLR4/MYD88, NFKB1, IL1B, IL6, TNF, CXCL8, CASP1) involved in innate sensing and inflammatory signaling.

3.4.4. Gene ontology (GO) enrichment analysis. To explore the functional relevance of the *Klebsiella*-related host-response targets potentially modulated by *E. tirucalli* L. constituents, Gene Ontology (GO) enrichment analysis was performed using STRING (v12.0). The analysis identified significant enrichment across Biological Process (BP), Cellular Component (CC), and Molecular Function (MF) categories (Table S2), yielding 23 enriched terms (Fig. 6). In the BP domain, the most enriched processes were strongly aligned with Gram-negative bacterial recognition and inflammation, including cellular response to molecules of bacterial origin, cellular response to lipopolysaccharide, response to lipopolysaccharide, and pattern

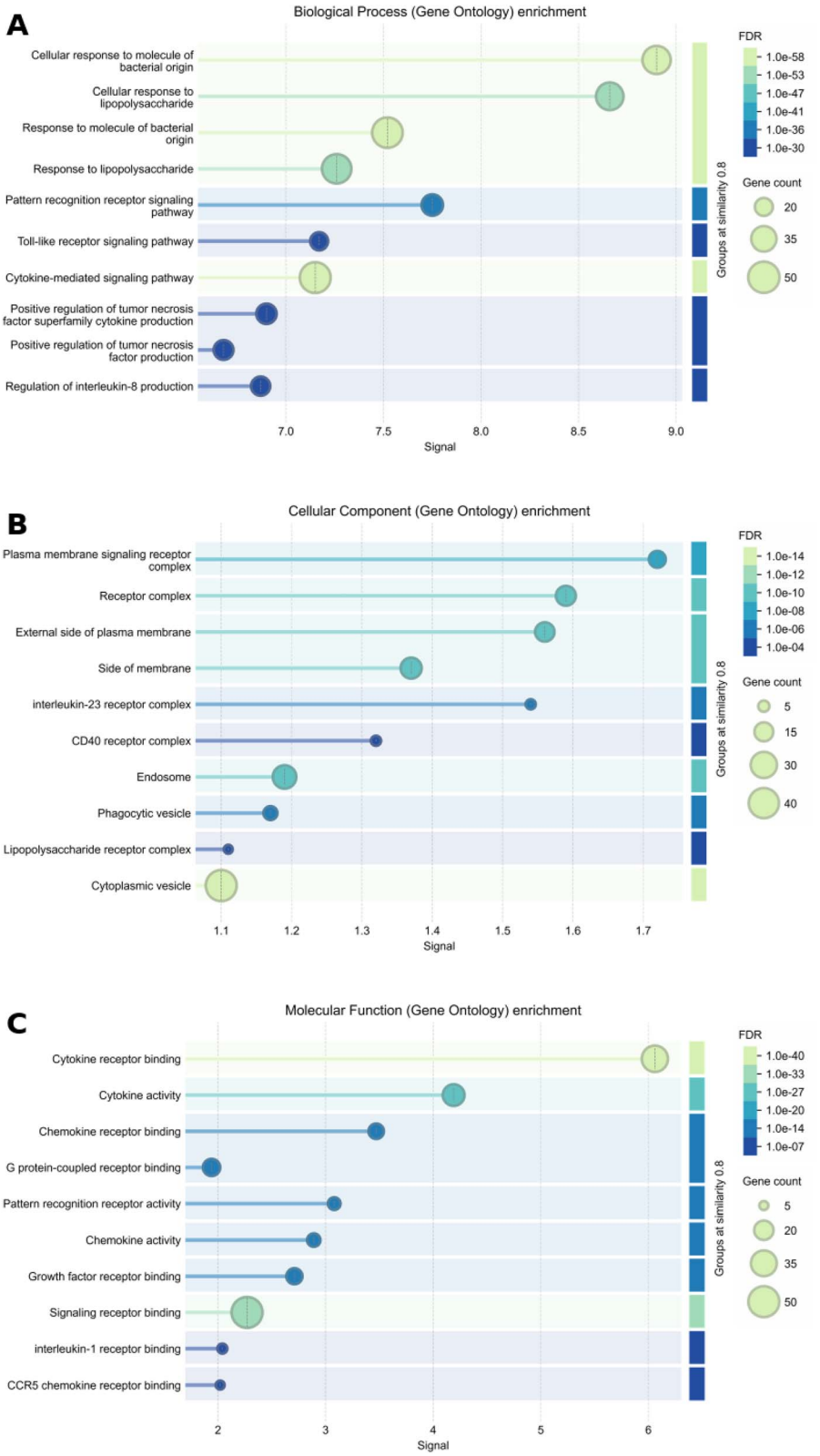

Fig. 6 Gene Ontology (GO) enrichment of *Klebsiella*-related host-response targets (STRING): (A) biological process terms dominated by responses to bacterial molecules/LPS and TLR signaling; (B) cellular component terms enriched for membrane receptor complexes, endosome/phagocytic vesicles; (C) molecular function terms enriched for cytokine/chemokine activity and receptor binding.

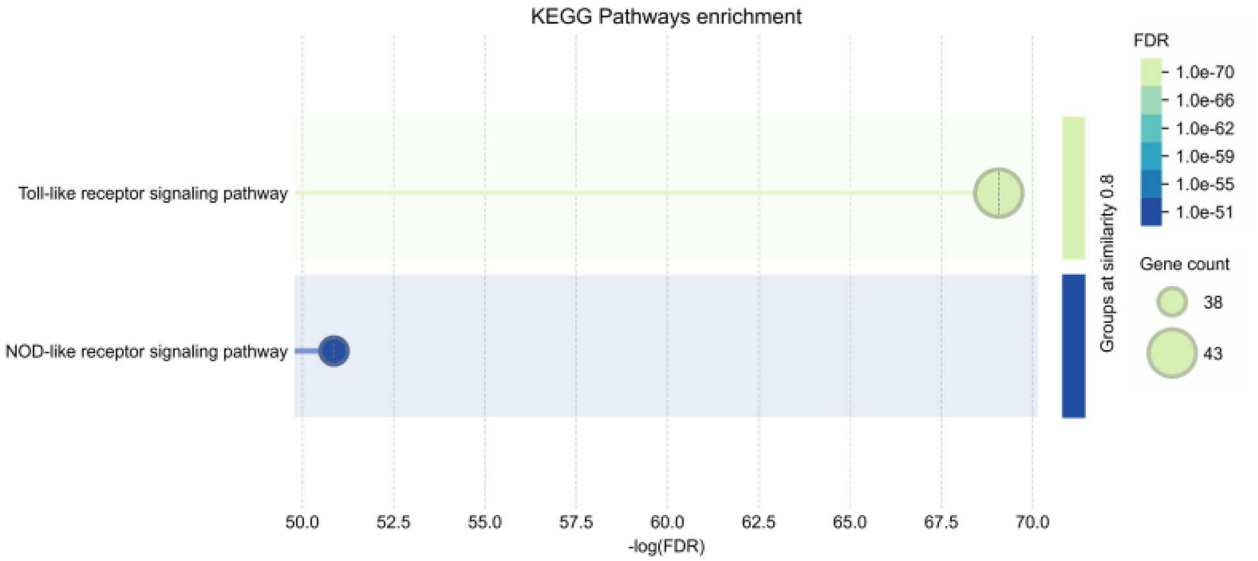

Fig. 7 KEGG pathway enrichment of *Klebsiella*-related host-response targets (STRING), highlighting significant enrichment of the Toll-like receptor and NOD-like receptor signaling pathways.

recognition receptor signaling and Toll-like receptor signaling, together with cytokine-mediated signaling and processes linked to TNF and IL-8 (CXCL8) production. These findings support that the curated target set is centered on host programs activated during *Klebsiella* infection, particularly LPS-driven innate immune activation and downstream inflammatory amplification. Consistent with this, CC terms were enriched for plasma membrane signaling receptor complexes, receptor complexes, and the external side of the plasma membrane, alongside endosome/phagocytic vesicle compartments and specific immune receptor assemblies such as the lipopolysaccharide receptor complex, interleukin-23 receptor complex, and CD40 receptor complex, highlighting membrane-proximal sensing and vesicular signaling hubs. In the MF category, enrichment was dominated by cytokine receptor binding/activity, chemokine activity and chemokine receptor binding, pattern recognition receptor activity, and broader signaling receptor binding, indicating that the network is functionally weighted toward immune mediator signaling and leukocyte recruitment mechanisms that shape antibacterial defense and inflammatory pathology in *Klebsiella* infection.

3.4.5. KEGG pathway enrichment analysis. To identify key signaling pathways associated with the *Klebsiella*-relevant host-response targets potentially modulated by *E. tirucalli* L. constituents, KEGG pathway enrichment analysis was performed using STRING (v12.0). The analysis revealed strong enrichment in two major innate immune pathways (Table S3 and Fig. 7): "Toll-like receptor signaling pathway" and "NOD-like receptor signaling pathway." These pathways represent central upstream frameworks for host detection of Gram-negative bacterial components and initiation of inflammatory defense programs. The TLR pathway enrichment is consistent with the presence of core LPS-sensing and adaptor nodes (*e.g.*, TLR4, CD14, LY96, MYD88, IRAK1/4, TRAF6, TICAM1/TIRAP) that couple pathogen recognition to activation of downstream transcriptional programs. In parallel, enrichment of the NOD-like receptor pathway aligns with intracellular sensing and inflammasome-linked signaling elements within the target set (*e.g.*, NOD1, NOD2, NLRP3, PYCARD, CASP1), supporting a mechanistic connection to cytokine maturation and inflammatory amplification during bacterial infection. Collectively, the KEGG findings indicate that the predicted target landscape of *E. tirucalli* metabolites is concentrated in pattern-recognition receptor (PRR) signaling axes that orchestrate antibacterial inflammation, leukocyte recruitment, and host defense responses relevant to *Klebsiella* infection outcomes.

The network pharmacology workflow in this study was designed specifically as a host-directed predictive analysis, using a manually curated seed panel of human proteins implicated in the immune and inflammatory response to *Klebsiella* infection. This framework is therefore distinct from the pathogen-directed docking analysis against bacterial LpxH, and the two are interpreted as complementary mechanistic layers rather than interchangeable explanations. Although the network pharmacology results highlight biologically plausible host pathways linked to Gram-negative infection, they remain predictive and require dedicated validation in appropriate cellular or *in vivo* models before any causal immunomodulatory conclusion can be drawn.

3.4.6. Molecular docking with *Klebsiella pneumoniae* LpxH (PDB ID: 8QK2). Molecular docking was conducted to investigate the binding interactions between key bioactive constituents isolated from *E. tirucalli* L. latex and UDP-2,3-diacylglucosamine hydrolase (LpxH) from *K. pneumoniae* (PDB ID: 8QK2). LpxH is a metalloenzyme in the lipid A/LPS biosynthesis pathway, and inhibition of this pathway is mechanistically relevant for Gram-negative bacteria, with no analogous LPS biosynthetic pathway in humans, making LpxH an attractive antibacterial target. The 8QK2 structure contains the co-crystallized ligand VTF (EBL-3339) and two catalytic Mn(II)

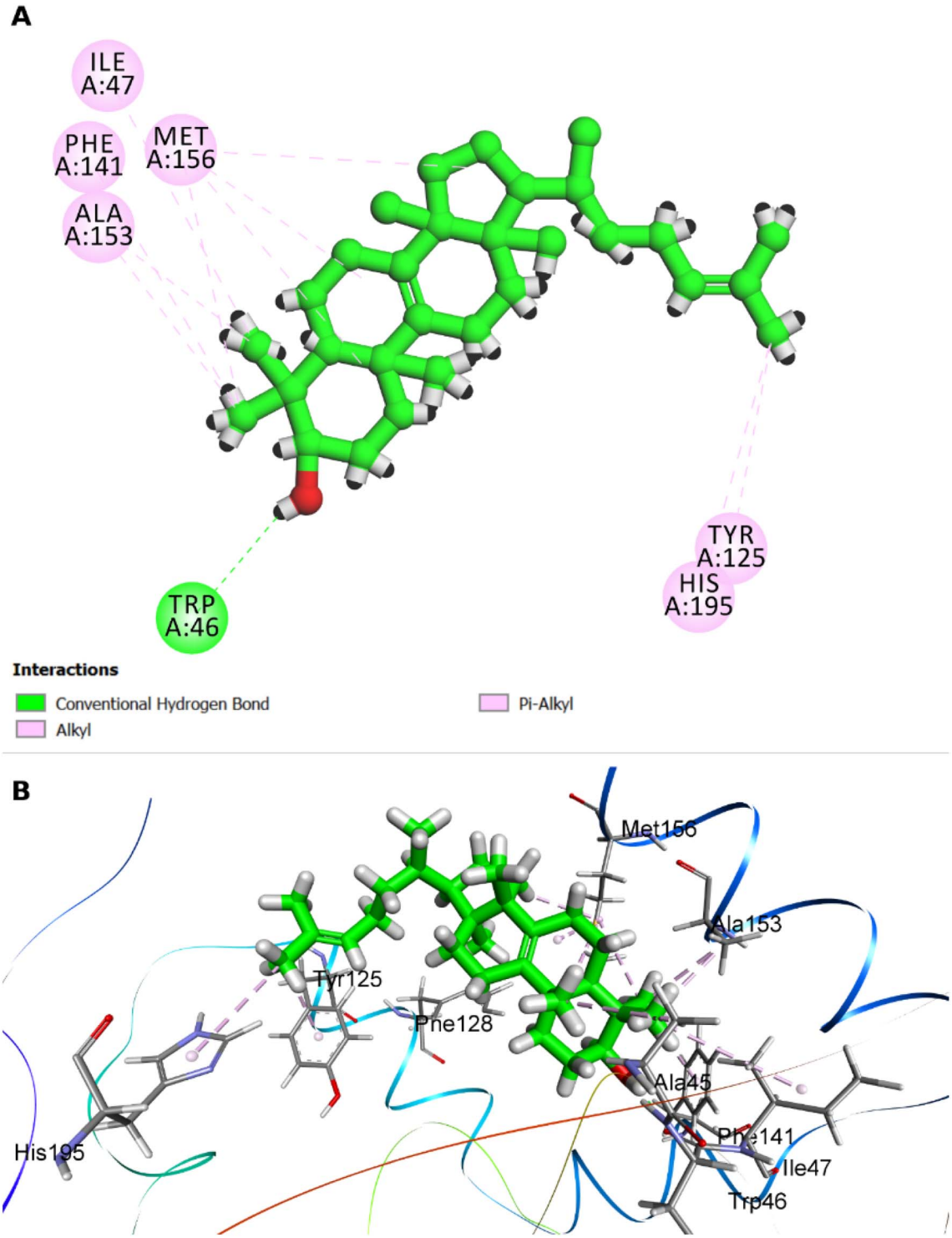

Fig. 8 2D (A) and 3D (B) interaction maps of the top-ranked *E. tirucalli* euphol docked into *K. pneumoniae* LpxH (PDB: 8QK2), showing a key H-bond (Trp46) and stabilizing alkyl/π-alkyl contacts (*e.g.*, Ile47, Phe141, Ala153, Met156, Tyr125, His195).

ions; accordingly, the docking search space was defined around the experimentally resolved ligand-binding pocket, and the crystallographic Mn(II) ions were retained as part of the rigid receptor to preserve the native metalloenzyme environment. Prior to docking, the protein was prepared by removing non-essential solvent molecules and unrelated heteroatoms, adding polar hydrogens, and converting the structure to PDBQT format using standard AutoDock-compatible preparation. The tested ligands (euphol, euph-8-enol, gallic acid, methyl gallate, and rutin) were geometry-optimized, protonated appropriately, and converted to PDBQT format. Docking was carried out using AutoDock Vina v1.2.5 with the grid centered on the co-

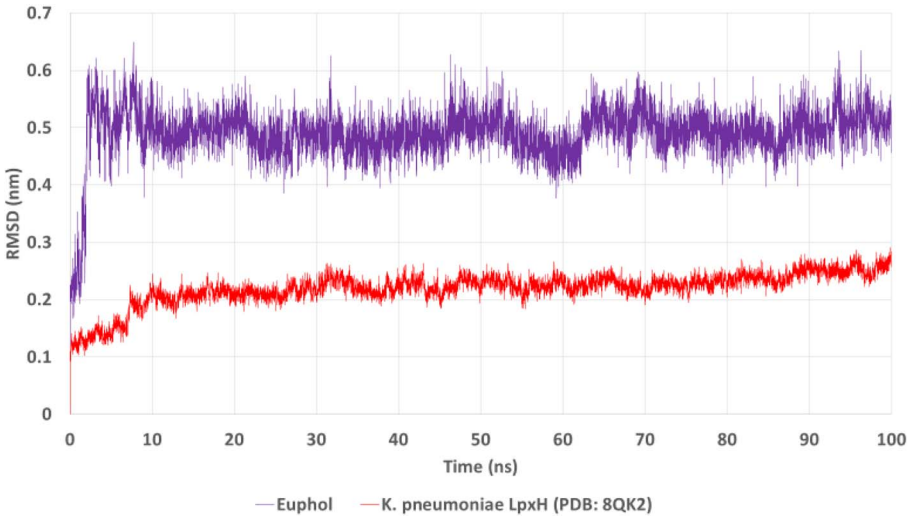

Fig. 9 RMSD analysis of the euphol-*K. pneumoniae* LpxH complex over 100 ns. Protein backbone RMSD (LpxH; red) indicates rapid equilibration and overall structural stability, while ligand RMSD (euphol; purple) reflects conformational/positional sampling within the binding pocket.

crystallized ligand-binding region and a grid box size of 24 × 24 × 24 Å. The exhaustiveness = 8, with up to 9 poses retained per ligand and an energy range of 3 kcal mol^{-1}. Binding affinity was reported (kcal mol^{-1}) of the top-ranked pose, and the final pose selection was based on both docking score and visual inspection of binding geometry using BIOVIA Discovery Studio Visualizer. To validate the docking protocol, the co-crystallized ligand VTF was extracted, prepared under the same workflow, and redocked into the original binding site; the redocked pose reproduced the crystallographic orientation with a RMSD of 1.03 Å, supporting the reliability of the adopted docking setup. Docking results are summarized in Table S4. Docking outcomes showed that euphol (**1**) achieved the strongest predicted affinity ($S = -8.13$ kcal mol; RMSD = 1.63 Å), followed by rutin (**5**) (−7.04; 1.02 Å). The remaining compounds displayed moderate binding: gallic acid (**3**) (−6.37; 1.57 Å), euph-8-enol (**2**) (−6.16; 1.61 Å), and methyl gallate (**4**) (−6.12; 1.69 Å). Overall RMSD values (1.02–1.69 Å) support consistent docking convergence across ligands. The 2D/3D interaction map (Fig. 8) was presented for euphol, which was the top-ranked ligand by docking score in our dataset, making it the most representative pose for discussing the strongest predicted binding mode in 8QK2. In addition, the euphol pose displayed a clear, interpretable interaction pattern in the binding pocket, combining a key hydrogen bond (Trp46) with multiple stabilizing hydrophobic (alkyl/π-alkyl) contacts (*e.g.*, Ile47, Phe141, Ala153, Met156, Tyr125, His195), which is consistent with highly lipophilic scaffold of euphol and supports a plausible pocket-anchoring mechanism. These binding features provide a plausible structural basis by which *E. tirucalli* metabolites could interfere with LpxH-dependent lipid A biosynthesis in *K. pneumoniae*.

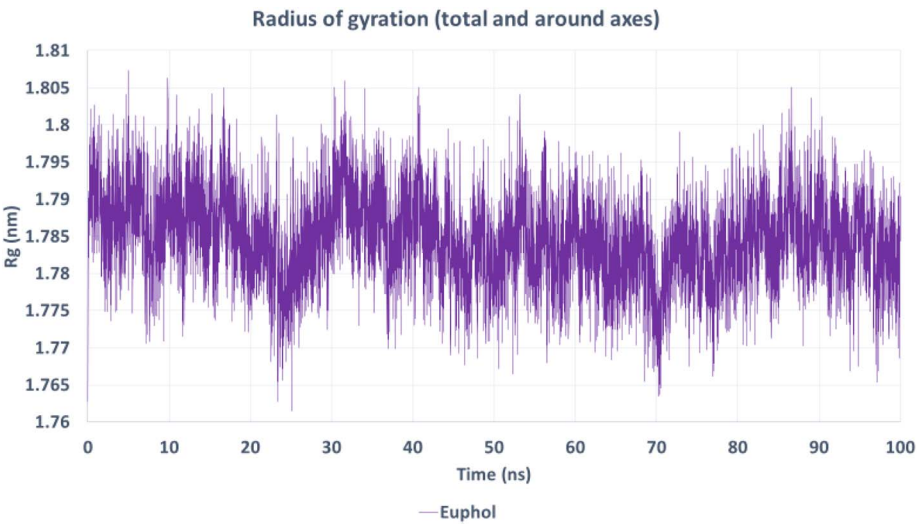

Fig. 10 Radius of gyration (R_g) of the euphol–LpxH complex during 100 ns MD. The nearly constant R_g indicates preserved compactness of LpxH throughout the simulation.

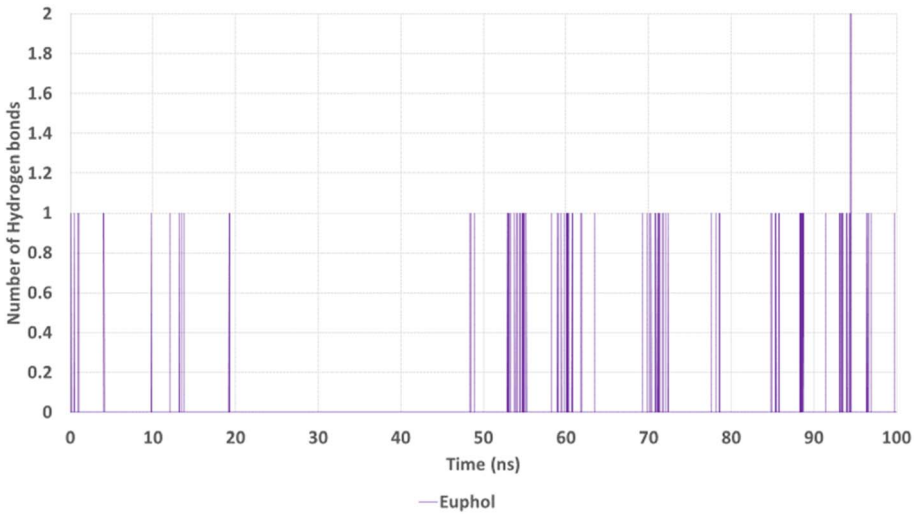

Fig. 11 Hydrogen-bond profile between euphol and LpxH during 100 ns MD. The intermittent 0–1 H-bond pattern suggests binding is dominated by hydrophobic packing with transient polar contacts.

3.4.7. Molecular dynamics (MD) simulation. To validate the docking-derived binding mode of euphol (**1**) and assess the dynamic stability of its complex with LpxH (8QK2) under explicit-solvent conditions. A single 100 ns production run was then performed without restraints, and coordinates were recorded every 10 ps. The MD analysis was intended as a qualitative structural stability assessment of the docked complex; therefore, trajectory evaluation focused on RMSD, radius of gyration (R_g), hydrogen-bond occupancy, RMSF, and potential energy.[26] Overall, the trajectory indicates a well-equilibrated protein scaffold with a stable global fold, while euphol exhibits moderate positional fluctuations that are consistent with a largely hydrophobic ligand exploring microstates within the binding cavity rather than maintaining persistent polar anchoring. The backbone RMSD of LpxH shows an early rise during the initial equilibration phase and then remains within a narrow low range (~0.12–0.28 nm) over the remainder of the simulation, with only a mild upward drift toward late time points (Fig. 9). Such behavior is typical of a protein reaching a stable conformational basin after relaxation from the starting structure. Notably, the absence of large-scale RMSD excursions supports that LpxH retains its overall fold throughout the 100 ns run, indicating that ligand binding does not induce destabilizing structural rearrangements at the global level. In contrast to the protein, euphol RMSD rapidly increases early in the trajectory and then fluctuates around a higher plateau (~0.45–0.60 nm). This pattern suggests that euphol undergoes reorientation and local diffusion within the pocket, as expected for a rigid, highly lipophilic scaffold dominated by van der Waals interactions. Importantly, the RMSD does not show runaway growth indicative of complete dissociation; instead, the trace supports continuous pocket residency with conformational sampling. This is consistent with the docking interaction profile.

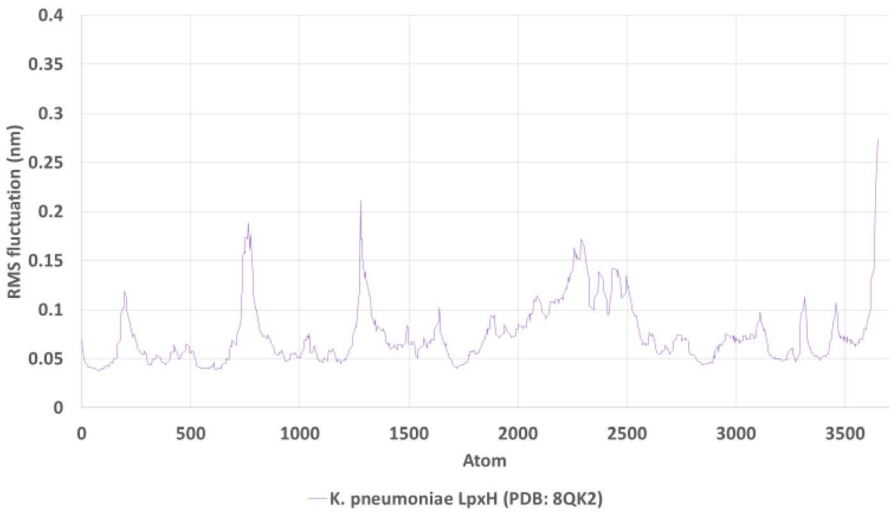

Fig. 12 Residue-wise RMSF of *K. pneumoniae* LpxH (8QK2) over 100 ns. Most residues show low fluctuations with localized peaks in flexible regions, supporting stable global folding.

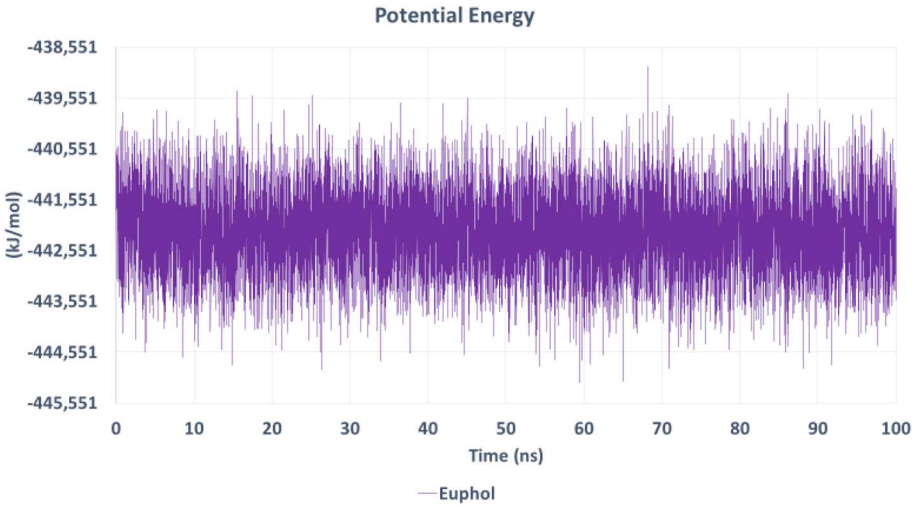

Fig. 13 Potential energy of the euphol–LpxH simulation system over 100 ns. Stable fluctuations around a constant mean indicate good energetic equilibration of the MD trajectory.

The radius of gyration remains tightly distributed (approximately 1.77–1.80 nm) without stepwise shifts or progressive expansion/contraction. This stability indicates that LpxH preserves overall compactness and does not undergo partial unfolding events during the simulation (Fig. 10). In practical terms, the stable R_g complements the low protein RMSD and supports that the system has reached structural equilibrium under the simulation conditions.

The hydrogen-bond profile between euphol and LpxH is sporadic, with the trajectory dominated by 0–1 hydrogen bonds and occasional transient spikes (rarely approaching 2). This is mechanistically coherent with euphol chemistry: the ligand contains limited polar functionality, so binding is expected to be driven primarily by hydrophobic packing and shape complementarity rather than persistent polar networks (Fig. 11).

The RMSF profile shows generally low fluctuations across most residues, with distinct peaks confined to flexible loop/terminal regions, a typical pattern for globular enzymes. The presence of higher RMSF at limited segments indicates that mobility is localized rather than global, supporting fold stability (Fig. 12). From a binding perspective, such flexible regions may contribute to breathing motions that allow euphol to sample alternative pocket microstates while the catalytic architecture remains largely preserved.

The potential energy trace shows stationary fluctuations around a consistent mean across the whole 100 ns window, without systematic drift. This behavior supports thermodynamic equilibration of the simulated system and indicates that the trajectory is suitable for qualitative stability assessment (Fig. 13). Stable potential energy, together with stable R_g and protein RMSD, strengthens confidence that the complex is not undergoing progressive destabilization.

Collectively, the MD results support a model in which the LpxH protein remains structurally stable and euphol maintains binding-pocket residency while dynamically exploring orientations and contact patterns within the cavity. The limited hydrogen-bond persistence suggests that binding is primarily mediated by hydrophobic packing, consistent with the docking interaction map and chemical properties of euphol. Therefore, the MD simulation provides dynamic support for euphol as a plausible LpxH-binding ligand, with stability expressed through maintained protein compactness and fold integrity, paired with ligand mobility typical of hydrophobic binders. Taken together, the data support a complementary host–pathogen mechanistic framework, in which *E. tirucalli* may influence infection outcome both by modulating host PRR-linked inflammatory responses and by directly targeting bacterial LpxH, thereby nominating its constituents as candidates for further validation in both antibacterial and mechanistic assays.

3.4.8. Limitation of the study. Despite the promising findings, future studies should focus on enzyme-based validation of LpxH inhibition, structure–activity relationship optimization, cytotoxicity evaluation, and *in vivo* efficacy studies to better establish the therapeutic potential of these compounds.

4. Conclusion

The phytochemical investigation of *E. tirucalli* latex led to the isolation and identification of five known compounds, four of which were identified in this species for the first time. Evaluation of their antimicrobial activities against *K. pneumoniae* (ATCC 13883), ESBL-producing *K. pneumoniae*, and carbapenem-resistant *K. pneumoniae* revealed potential starting points for the development of anti-*Klebsiella* agents. Methyl gallate (**4**) exhibited remarkable activity against *K. pneumoniae* (ATCC 13883) with an MIC of 0.01 mM, while euphol (**1**) was the most effective against ESBL *K. pneumoniae* (MIC = 13.12 mM). Notably, euph-8-enol (**2**) demonstrated the highest potency against carbapenem-resistant *K. pneumoniae* (MIC = 0.69 mM). The integrated network pharmacology analysis indicated that *E. tirucalli* constituents could modulate a focused set of host-response proteins and pathways that govern Gram-negative bacterial recognition and inflammatory signaling, including

TLR/NOD-driven innate activation, cytokine/chemokine communication, inflammasome-associated processes, complement amplification, and oxidative antimicrobial defense. Molecular docking against *K. pneumoniae* LpxH (PDB: 8QK2), an essential enzyme in lipid A/LPS biosynthesis, demonstrated favorable binding scores across the tested metabolites, with euphol (-8.13 kcal mol^{-1}) showing the strongest predicted affinity. Molecular dynamics simulations of the euphol–LpxH complex further supported the structural feasibility of binding by revealing stable protein behavior, preserved compactness, and thermodynamic equilibration over the 100 ns trajectory, consistent with sustained ligand accommodation primarily through hydrophobic packing. These findings provide a mechanistic framework supporting *E. tirucalli* as a potential starting point for future antibacterial optimization for anti-*Klebsiella* lead discovery and justify future experimental validation, including enzyme inhibition assays (LpxH/LPS pathway), antibacterial testing against resistant *Klebsiella* strains, and *in vivo* efficacy and safety studies.

Author contributions

Conceptualization: U. R. A., F. A. B.; methodology: R. M. A., M. A. M., M. E. R., R. I. B., H. A. A., A. H. E.; software: R. M. A., M. A. M., R. I. B., H. A. A., M. E. R., A. H. E.; formal analysis: R. M. A., M. A. M., M. E. R., R. I. B., H. A. A., A. H. E.; investigation: U. R. A., F. A. B.; resources: U. R. A., F. A. B.; data curation: U. R. A., F. A. B.; writing–original draft: R. M. A., M. A. M., R. I. B., H. A. A., A. H. E.; writing–review and editing: U. R. A., M. E. R.; supervision: U. R. A. All authors have read and agreed to the published version of the manuscript.

Conflicts of interest

The authors declare no conflict of interest.

Data availability

All data generated in this research work are available at the supplementary information (SI) provided with the manuscript. Supplementary information is available. See DOI: https://doi.org/10.1039/d6ra00720a.

Acknowledgements

We thank Deraya University for supporting this work. The authors extend their appreciation to the Deanship of Research and Graduate Studies at King Khalid University for funding this work through a small group research project under grant number RGP1/68/46.

References

1 R. Benjamaa, A. Moujanni, N. Kaushik, E. H. Choi, A. K. Essamadi and N. K. Kaushik, *Front. Plant Sci.*, 2022, **13**, 1008881.
2 P. Y. Mali and S. S. Panchal, *Asian Pac. J. Trop. Biomed.*, 2017, **7**, 603–613.
3 D. Chang, L. Sharma, C. S. Dela Cruz and D. Zhang, *Front. Microbiol.*, 2021, **12**, 750662.
4 C. Liu and J. Guo, *Ann. Clin. Microbiol. Antimicrob.*, 2019, **18**, 4.
5 S. Navon-Venezia, K. Kondratyeva and A. Carattoli, *FEMS Microbiol. Rev.*, 2017, **41**, 252–275.
6 B. Li and T. J. Webster, *J. Orthop. Res.*, 2018, **36**, 22–32.
7 L. K. Logan and R. A. Weinstein, *J. Infect. Dis.*, 2017, **215**, S28–S36.
8 H. Ganshirt, , M. Brenner, H. Bolliger and E. Stahl*et al.*, *Thin-layer Chromatography; a Laboratory Handbook*, Springer-Verlag, 1965.
9 T. Al-Warhi, E. M. Zahran, S. Selim, M. M. Al-Sanea, M. M. Ghoneim, S. A. Maher, Y. A. Mostafa, F. Alsenani, M. A. Elrehany and M. S. Almuhayawi, *Antioxidants*, 2022, **11**, 881.
10 A. H. Elmaidomy, U. R. Abdelmohsen, F. Alsenani, H. F. Aly, S. G. E. Shams, E. A. Younis, K. A. Ahmed, A. M. Sayed, A. I. Owis and N. Afifi, *RSC Adv.*, 2022, **12**, 11769–11785.
11 A. H. Elmaidomy, E. M. Zahran, R. Soltane, A. Alasiri, H. Saber, C. J. Ngwa, G. Pradel, F. Alsenani, A. M. Sayed and U. R. Abdelmohsen, *Molecules*, 2022, **27**, 5617.
12 H. T. Bakhsh, F. A. Mokhtar, A. H. Elmaidomy, H. F. Aly, E. A. Younis, M. A. Alzubaidi, F. H. Altemani, N. A. Algehainy, M. A. A. Majrashi and F. Alsenani, *Plants*, 2023, **12**, 2382.
13 E. M. Mohamed, A. H. Elmaidomy, R. Alaaeldin, F. Alsenani, F. H. Altemani, N. A. Algehainy, M. A. Alanazi, A. Bagalagel, A. Althagafi and M. A. Elrehany, *Metabolites*, 2023, **13**, 732.
14 A. H. Elmaidomy, S. A. Mohamad, M. Abdelnaser, R. Yahia, F. A. Mokhtar, F. Alsenani, M. Y. Badr, S. Y. Almaghrabi, F. H. Altemani and M. A. Alzubaidi, *Food Funct.*, 2023, **14**, 7156–7175.
15 T. S. Alnusaire, A. M. Sayed, A. H. Elmaidomy, M. M. Al-Sanea, S. Albogami, M. Albqmi, B. F. Alowaiesh, E. M. Mostafa, A. Musa and K. A. Youssif, *Antioxidants*, 2021, **10**, 1860.
16 H. T. Bakhsh, O. H. Abdelhafez, A. H. Elmaidomy, H. F. Aly, E. A. Younis, M. A. Alzubaidi, N. A. Algehainy, F. H. Altemani, M. Majrashi and F. Alsenani, *Beni-Suef Univ. J. Basic Appl. Sci. Journal of Basic and Applied Sciences*, 2024, **13**, 1.
17 S. Samir, F. A. Behery, M. A. Zarka, R. I. Bedaiwi, H. A. Abou-Zied, U. R. Abdelmohsen, R. M. Abd El-Baky, M. A. Mawhoup, M. Mahrous and R. E. Abdelnaem, *PLoS One*, 2025, **20**, e0338733.
18 CLSI, *Performance Standards for Antimicrobial Susceptibility Testing*, Clinical and Laboratory Standards Institute, Wayne, PA, 2024.
19 C. Von Mering, L. J. Jensen, B. Snel, S. D. Hooper, M. Krupp, M. Foglierini, N. Jouffre, M. A. Huynen and P. Bork, *Nucleic Acids Res.*, 2005, **33**, D433–D437.
20 P. Shannon, A. Markiel, O. Ozier, N. S. Baliga, J. T. Wang, D. Ramage, N. Amin, B. Schwikowski and T. Ideker, *Genome Res.*, 2003, **13**, 2498–2504.
21 F. A. Behery, M. A. M. El Gendy, M. A. Zarka, M. A. Alzubaidi, H. A. Abou-Zied, G. Bringmann, U. R. Abdelmohsen and A. H. Elmaidomy, *Sci. Rep.*, 2025, **15**, 32595.

22 T. A. Beu and A. Farcaş, *J. Comput. Chem.*, 2017, **38**, 2335–2348.
23 V. A. Nyigo, X. Peter, F. Mabiki, H. M. Malebo, R. H. Mdegela and G. Fouche, *J. Phytopharmacol.*, 2016, **5**, 100–104.
24 L. M. López-Martínez, H. Santacruz-Ortega, R.-E. Navarro, R. R. Sotelo-Mundo and G. A. González-Aguilar, *PLoS One*, 2015, **10**, e0140242.
25 T. Pivec, R. Kargl, U. Maver, M. Bračič, T. Elschner, E. Žagar, L. Gradišnik and K. Stana Kleinschek, *Polymers*, 2019, **11**, 1566.
26 E. R. Abdelaleem, H. A. Abou-Zied, C. J. Ngwa, M. E. Rateb, U. R. Abdelmohsen and A. A.-R. Gomaa, *S. Afr. J. Bot.*, 2025, **184**, 337–348.